Light scattering regimes along the optical axis in turbid media

S. D. Campbell, A. K. O'Connell, S. Menon, Q. Su, and R. Grobe
Intense Laser Physics Theory Unit and Department of Physics, Illinois State University, Normal, Illinois 61790-4560, USA
(Received 14 March 2006; published 26 December 2006)

We inject an angularly collimated laser beam into a scattering medium of a nondairy creamer-water solution and examine the distribution of the scattered light along the optical axis as a function of the source-detector spacing. The experimental and simulated data obtained from a Monte Carlo simulation suggest four regimes characterizing the transition from unscattered to diffusive light. We compare the data also with theoretical predictions based on a first-order scattering theory for regions close to the source, and with diffusionlike theories for larger source-detector spacings. We demonstrate the impact of the measurement process and the effect of the unavoidable absorption of photons by the detection fiber on the light distribution inside the medium. We show that the range of validity of these theories can depend on the experimental parameters such as the diameter and acceptance angle of the detection fiber.

DOI: 10.1103/PhysRevE.74.061909 PACS number(s): 87.90.+y, 05.60.−k, 42.62.Be

I. INTRODUCTION

The propagation of particles and radiation in highly scattering media has been studied extensively for several decades [1–3]. Direct applications can be found in areas of science and technology including, e.g., reactor physics, meteorology, astrophysics, oceanography, diffusive light imaging, and quality control in manufacturing [4–6]. In the past few years, this research has witnessed the progress reported in bio-optical imaging using lasers in the near infrared region, for which the medium's absorption is negligible compared to its scattering strength. The goal in the latter studies is to use the scattered light to reconstruct the optical parameters that characterize the medium.

There are three main types of approaches to examine the scattering properties of diffusive media using laser fields. The first two types measure the light outside the medium. These include reflectance measurements and transmission studies of samples with a finite size [7]. These are ideal measurements as the detection process itself has no impact on the light distribution inside the medium. Here a theoretical description of the observed data does not require the inclusion of the absorption due to the measurement. The third type of approach involves the observation of the light inside the medium where the data can be obtained as a function of the position of the optical detection fiber [8,9]. In this case the measurement could be destructive to the scattered light thus requiring the details of the measurement process to be included in the prediction of the data.

To the best of our knowledge, nearly all light scattering experiments were performed in the nondestructive measurement regime. In many cases, the studies have used isotropic sources located deep inside the medium to generate a spherically symmetrical illumination. This approach has three main advantages. First, the theoretical modeling based on the diffusion approximation provides simple and fully analytical solutions even for pulsed or intensity modulated light and, second, the theoretically difficult to describe few-scattering events that dominate the light distribution close to the source are not so important making the diffusion theory valid for shorter distances [10,11]. Third, only a minor fraction of the isotropically ejected light is removed by the detection fiber.

In other situations of angularly collimated beams, the source-detector (*s-d*) spacing was chosen so large that light was already highly diffusive and the loss due to the detected photons relative to the available photons in that region was very small. In this large-distance region in which most experimental light-scattering studies were carried out, good agreement was found with diffusionlike theories. However, in this regime the scattering data depend only on the reduced scattering coefficient which makes a recovery of the full set of scattering parameters problematic [10,11].

In this work, we examine theoretically and also experimentally scattered light from an angularly collimated source and study its distribution along the optical axis covering the entire range from the ballistic (beamlike) regime to the diffusion regime. This on-axis region is important as it is the location where light is brightest and therefore most promising for imaging. In contrast to measurements either outside the medium or off-axis and inside the medium, the on-axis detection of light inside the medium can be difficult to model theoretically. For example, there are no known analytical expressions that describe the transition region between ballistic and diffusion, and the very process of detecting photons from the beam can have a direct impact on the light distribution. In other words, depending on the *s-d* spacing the measurement could change from ideal (no impact on the distribution) to destructive. In general, theories to predict the data in destructive measurements are nontrivial to come by as the local effect of a perfect absorber (the detector) has to be taken into account.

We should point out that in the on-axis domain the realm of validity of the theories with regard to the *s-d* spacing can depend on how the light is detected by the fiber. For instance, we will show below that the larger the numerical aperture and diameter of the detection fiber, the shorter the *s-d* spacing at which the diffusion theory becomes valid. On the other hand, large numerical apertures and fiber diameters limit the applicability region of few-scattering theories to only small *s-d* spacings.

The interaction of light with turbid media has been intensively studied and the present theoretical and experimental

work relies in several aspects on previous studies [3]. For example, some works have explored the transition between the various scattering regimes depending on the source-detector spacings. The principal theoretical problem here is to find a unified theory that can satisfactorily describe all four intensity regions. As a recent example, You and collaborators [12] have explored the possibility of using a modified scattering phase function to better match the transition from the ballistic and transport to the diffusive regimes. In this study the δ-P_1 approximation [13,14] permitted a better accuracy for small source detector spacings than the usual diffusion theory. Other studies have focused on the modification of the intensity behavior for very small detector source spacings [15–20] and showed that the light depends on the details of the collection fiber. In none of these works, however, was the effect of the absorption of the fiber with regard to the measured intensity taken into account.

We also note that most experiments used larger concentrations of scattering agents [21,22] which does not allow a clean separation between the various scattering regimes to be measured. For example, the several studies based on intralipid with various concentrations focused on the diffusive regime that is characterized by inverse scattering lengths that are often smaller than 1 mm. As a result the exponential-falloff regime as well as the entry region discussed in this work could not be resolved spatially as the main focus was more on the diffusive regime. Even though many experiments scanned an optical fiber through a tank with a highly scattering medium, we are not aware of experimental data that use systematic measurements of the transverse beam profile to determine the light distribution along the optical axis for relatively dilute media.

The paper is organized as follows. In Sec. II we introduce the four distinct spatial regimes with regard to the *s*-*d* spacing. A detection of on-axis light requires a discussion about the potential impact of the measurement on the light distribution. Based on a Monte Carlo simulation to the Boltzmann equation we show under which conditions on-axis measurements are nondestructive. In Sec. III we discuss a few-scattering theory and establish its range of validity for the first two intensity regimes. In Sec. IV we study the validity of diffusive theories. In Sec. V we show how the four regimes can be used together to reconstruct the scattering coefficients for our experimental data. We illustrate this by analyzing our experimental scattering data obtained for a diluted solution of nondairy creamer in water. We conclude with a brief discussion and outlook.

II. FOUR SPATIAL REGIMES OF INTENSITY

In the absence of coherent wave effects [23,24], the steady state distribution for laser light in a highly scattering medium can be described by the Boltzmann (radiative transfer or transport) equation [2] for the irradiance $I(\mathbf{r},\mathbf{\Omega})$ as a function of the position $\mathbf{r}$ and the propagation direction $\mathbf{\Omega}$ (with $\mathbf{\Omega}^2=1$):

$$\mathbf{\Omega}\cdot\nabla I(\mathbf{r},\mathbf{\Omega}) = -(\mu_s+\mu_a)I(\mathbf{r},\mathbf{\Omega}) + \mu_s\int d\mathbf{\Omega}' p(\mathbf{\Omega},\mathbf{\Omega}')I(\mathbf{r},\mathbf{\Omega}') + S(\mathbf{r},\mathbf{\Omega}), \tag{2.1}$$

where $\mu_s(\mu_a)$ is the scattering (absorption) coefficient. The incoming light can be either modeled via an appropriate boundary condition or by a source term $S(\mathbf{r},\mathbf{\Omega})$. The conditional probability that an incoming photon with (normalized) velocity $\mathbf{\Omega}'$ is scattered into the $\mathbf{\Omega}$ direction is denoted by the scattering phase function $p(\mathbf{\Omega}\cdot\mathbf{\Omega}')$ which we model here by the Henyey-Greenstein phase function, $f_{\mathrm{HG}}(\mathbf{\Omega}\cdot\mathbf{\Omega}')\equiv(1-g^2)/\{4\pi(1+g^2-2g\mathbf{\Omega}\cdot\mathbf{\Omega}')^{3/2}\}$, where the anisotropy parameter g is the average cosine of the scattering angle $g\equiv\langle\mathbf{\Omega}\cdot\mathbf{\Omega}'\rangle$. We assume that the medium has a length W and that the (narrow) laser beam is injected into the medium at $\mathbf{r}=(0,0,0)$ along the z direction, $S(\mathbf{r},\mathbf{\Omega})\equiv\delta(\mathbf{r})\delta(\mathbf{\Omega}-\mathbf{e}_z)$. In our theoretical analysis we also assume for simplicity that the medium is index matched such that there are no surface-induced reflections associated with the interfaces at $z=0$ and $z=W$.

In this work we locate the detection fiber along the optical beam axis at $\mathbf{r}=(0,0,z)$. It is characterized by a circular surface area of radius ρ_D and a maximum acceptance cone (field of view) with half angle α_D that is directly related to the fiber's numerical aperture and the index of refraction of the medium. Except for the more general derivation in Sec. III, we assume that the orientation of this fiber, $\mathbf{n}_D$, is parallel to the optical axis, $\mathbf{n}_D=\mathbf{e}_z$.

As solutions that describe the intensity distribution $I(\mathbf{r},\mathbf{\Omega})$ for a wide range of parameters are very difficult to obtain analytically, we have performed large scale Monte Carlo simulations [25–32] to the Boltzmann equation based on up to 10^8 photons that were injected at $\mathbf{r}=0$ into the medium. Due to the independence of each random path, parallel computations could be performed on Xgrid, a distributed computing architecture for a cluster of 27 Macintoshs with cycle rates of 0.7 to 2.7 GHz. Each photon performed a random walk [32] with a random distance s distributed according to $P(s)=\mu_s\exp(-\mu_s s)$ and with a random scattering angle according to $f_{\mathrm{HG}}(\mathbf{\Omega}\cdot\mathbf{\Omega}')$. Due to the required large number of photons and scattering events the usual random number generators based on the linear congruence method with a period of 2×10^9 was not appropriate [31]. We found better and less correlated quasirandom numbers using the Kirkpatrick-Stoll r250 algorithm [33] that is based on a fast shift register generator and has a period of more than 10^{74}.

Photons that passed through a circular disk of radius ρ_D centered at $\mathbf{r}=(0,0,z)$ were counted if their incoming angle with the detector's normal $\mathbf{n}_D$ direction was less than the angle α_D. To account for absorption (used in Sec. V), each photon was weighted according to the factor $\exp(-\mu_a L)$, where L denotes the total length of each photon path. From now on (except in Sec. V), we will take advantage of the scaling property of the Boltzmann equation and use μ_s^{-1} as the unit of length.

Let us now discuss how the intensity falls off along the optical axis as a function of the detection parameters. In Fig.

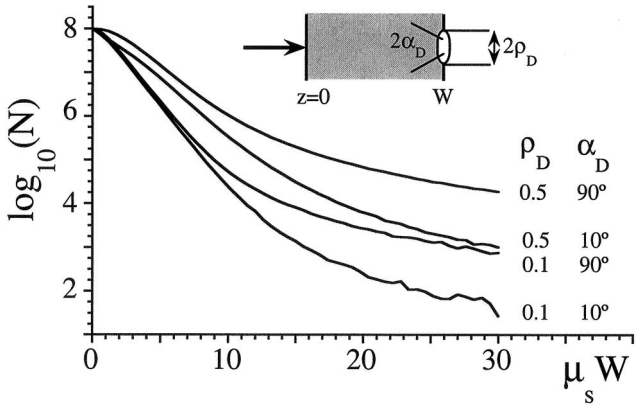

FIG. 1. Transmitted light intensity detected at circular area with radius ρ_D and field of view α_D as a function of the width of the slab W. The detector is located at the exist surface ($x=0$, $y=0$, and $z=W$). ($N=10^8$ injected photons; $\mu_s=1$; $\mu_a=0$; $g=0.9$.)

1 we display the detected light intensity as a function of the distance to the detector z which we chose here to be at the exit surface of the medium of length W with $\mu_s=1$, $\mu_a=0$, and $g=0.9$. In each of the four simulations, we have injected $N=10^8$ photons into the entry surface of the medium and counted the photons that passed through the detector. The four curves correspond to $\rho_D=0.1$ and 0.5 and $\alpha_D=10°$ and 90° to represent various fibers with different numerical apertures. Due to the choice $z=W$ each photon can pass the detection area only once.

We observe four distinct regimes. The first regime (I) for very short distances (for our detection parameters $z<2$) is characterized essentially by light that did not have the opportunity to scatter very often. For a wide field of view of the detector (close to 90°) the intensity decay curve starts with a vanishing slope. Note that in this thin slab regime the detected transmission depends very sensitively on the parameters of the fiber. One could also expect [34] that this regime also depends most sensitively on the choice of the scattering phase function. It is important to note that in contrast to the Beer-Lambert law [15–20], this regime is not exponential and its initial slope depends quite sensitively on g, ρ_D, and α_D.

The next and potentially most interesting regime (II) ($2<z<10$) is characterized by a nearly exponential decay that, in the case of the smallest detector ($\rho_D=0.1$ and $\alpha_D=10°$), extends to nearly four orders of magnitude in intensity. We note that the exponential decay rate in this regime depends on the parameters of the fiber, e.g., the slope is steepest for $\rho_D=0.1$ and $\alpha_D=10°$. Also the spatial extension of this exponential regime depends on the fiber. This extension is longest for $\rho_D=0.1$ and $\alpha_D=10°$ and shortest for $\rho_D=0.5$ and $\alpha_D=90°$.

Regime III ($10<z<25$) describes the transition from few scattering to the diffusive behavior. For the longest distances we enter the diffusion regime IV ($25<z$) that has been most thoroughly studied in the literature.

In order to obtain a more quantitative understanding of these four regimes along the optical axis, we will discuss below some analytical approaches and compare their predictions systematically with the Monte Carlo (MC) data. Before we do this, however, it is important to comment on the impact of the measurement process on the light distribution for the experimental situation discussed in Sec. V where the medium has a fixed length W and the detector is inside the medium, $z<W$. For instance, for small detection distances z nearly all photons that would otherwise brighten the medium are absorbed by the fiber. This blocking of the beam could therefore influence the light distribution in the entire medium and even modify the light that would be at location z in the absence of any detection. The effect of the detection fiber can be modeled by adding a spatially localized component to the absorption coefficient, allowing for the photons to be fully absorbed if they pass through the circular surface area of the detector, centered at location $\mathbf{r}$. However, this approach does not describe accurately those photons that suffer an unavoidable reflection at the surface of the fiber due to an index mismatch. It also removes those photons from the dynamics whose incoming angle is larger than the field of view of the fiber and therefore are not detected.

We define a measurement to be destructive if a photon that passes through the area of the detector can return to the detector. This second passage contributes obviously to the real light distribution at that location but it cannot be measured if the photon was absorbed during its first passage through the detection area. In order to determine quantitatively the importance of this effect due to the measurement, we have introduced a parameter Ξ, as a degree of destructiveness of the measurement. It is natural to define it as the number of returned passages through the detector opening relative to the number of photons that pass through it, $\Xi \equiv$(total number of returns)/(number of photons).

In Fig. 2(a) we show the behavior of this parameter Ξ for two fibers with detection radius $\rho_D=5$ and $\rho_D=10$ (and $\alpha_D=90°$) as a function of the location of the fiber z for two media of length $W=50$ and 100. For comparison, in Fig. 2(b) we show also the number of detected photons among the total of 10^8. For the larger detector area, $\rho_D=10$, Ξ reaches its maximum value (here around 10%) in the middle region of the medium, $z\approx 0.5W$, meaning that any theory that does not include the absorptive effect of the measurement would overestimate the experimental data by 10%.

The small value of Ξ close to $z\approx 0$, where the light beam is injected, might seem counterintuitive at first. Even though this is the region where the fiber absorbs nearly all photons and therefore blocks the entire beam for the rest of the medium, $\Xi\approx 0$ suggests a nondestructive measurement. The reason for this surprising result is related to the entry surface at $z=0$, which is nonreflective as we have assumed an index matched interface. In order to be detected for a second time, the photons would have to turn around after their first passage through the detector area. These reversed photons would have to pass the $z\approx 0$ plane first and then turn around again to be able to reenter the fiber. However, these photons do not have enough scattering space available; they would cross the interface at $z=0$ and therefore can never return to the fiber. The same mechanism explains also why Ξ reduces to zero at the other interface at $z\approx W$.

Comparing the two values for Ξ for the wide and narrow detectors, it is clear that the measurement is potentially de-

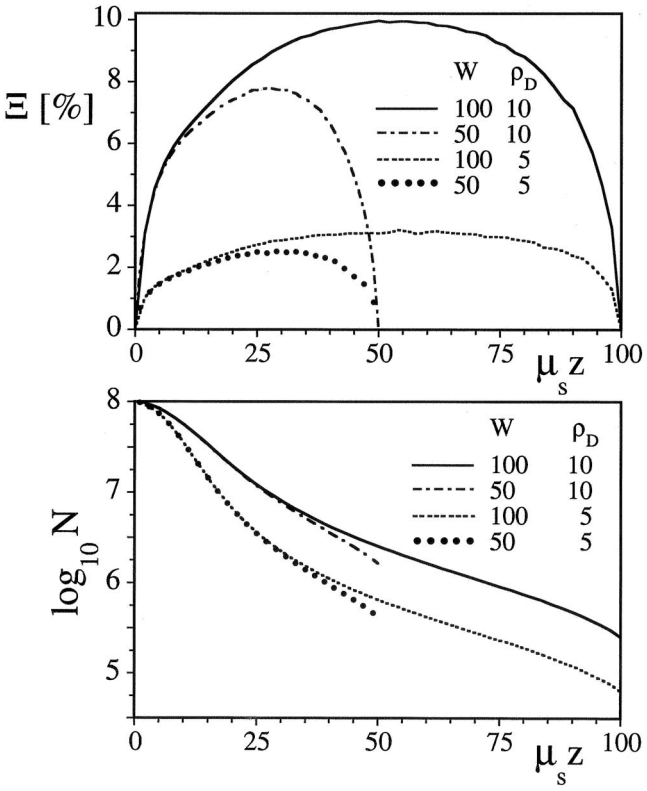

FIG. 2. The degree of destructiveness Ξ as a function of the location of the detector z for a wide and narrow detection with fiber radii $\rho_D=5$ and 10. The parameter Ξ is related to the ratio of the (at least) doubly to singly detected photons. The bottom graph shows the number of detected photons as a reference. [$N=10^8$ photons, $\alpha_D=90°$, $\mu_s=1$, $\mu_a=0$, $g=0.9$, $W=100$, and $W=50$ (dashed line).]

structive only for large media and significantly large fiber areas $\pi{\rho_D}^2$. This is expected as the return probability for a photon decreases with decreasing detector area. The other two curves were obtained for a shorter medium ($W=50$) and suggest that the maximum value of Ξ can increase with increasing width W as more photons have the opportunity to return to z before exiting the medium at W. For an experimental setup (discussed in Sec. V) the degree of destructiveness Ξ is a key parameter to determine a sufficiently small detector area to maximize the agreement with theories that do not take the removal of the measured photons into account.

In the next section we will describe various theoretical attempts to model these individual four regions discussed in Fig. 1. In Sec. V we will compare the theoretical predictions with experimental data. In contrast to the comparison with the Monte Carlo simulation where all parameters can be easily controlled, in the experimental situation we have control only over the detection parameters ρ_D and α_D, requiring a fitting for the scattering parameters such as μ_s, g, and μ_a.

III. FIRST-ORDER SCATTERING THEORY FOR REGIMES I AND II

In order to have an analytical description for the light distribution close to the source, let us discuss the prediction

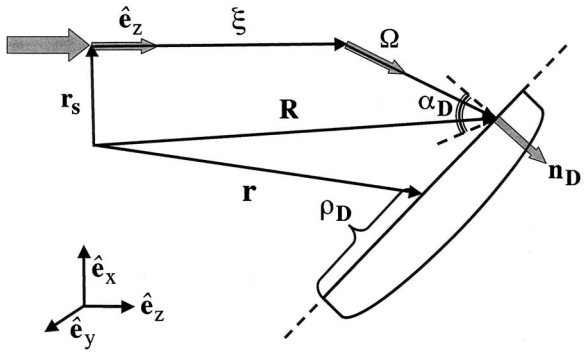

FIG. 3. Geometry and parameters for the single-scattering regime.

of a simplified approach in which we assume that only unscattered and singly scattered light contributes to the detected signal. We also assume that the laser beam's initial divergence is negligible. Neglecting any coherence properties of the beam there are two regimes of interest depending on the ratio of the diameters of the detection fiber and the initial beam.

Let us study the case in which the beam's initial diameter is much narrower than that of the detection fiber. The opposite limit can be obtained by integrating the result over various "narrow" beams. In Fig. 3 we have sketched the relevant parameters that can be chosen more generally than discussed in the previous section. We assume that the light is injected at location $\mathbf{r}_s \equiv (x_s, y_s, 0)$ with a velocity parallel to the z axis, traveling to location $\mathbf{r}_s+\boldsymbol{\xi}$, with $\boldsymbol{\xi} \equiv (0,0,\xi)$, before it gets scattered. The detection fiber is placed at $\mathbf{r} \equiv (x,y,z)$, its radius is ρ_D, its orientation is given by the unit vector $\mathbf{n}_D$, and its maximum acceptance angle is α_D. The vector $\mathbf{R}(\boldsymbol{\xi},\boldsymbol{\Omega}) \equiv (X,Y,Z)$ denotes the location where the photon with a direction given by the unit vector $\boldsymbol{\Omega}$ would pass through the plane spanned by the detector area. In this approach the detected light is proportional to sum of two contributions: The unscattered light whose probability is denoted by $D_0(\mathbf{r})$ and the probability due to singly scattered light $D_1(\mathbf{r})$.

The probability to detect unscattered light is only nonzero along the optical axis and it is given by the (infinite) product of the probabilities not to scatter or absorb within the interval of length $\Delta\xi=z/K$ (where K denotes the number of intervals), leading to $\Pi_n[1-(\mu_s+\mu_a)\Delta\xi] \rightarrow \exp[-(\mu_s+\mu_a)z]$. As a result, its contribution to the detected light is

$$D_0(\mathbf{r}) = \exp[-\mu_T z]\Theta[{\rho_D}^2 - (x-X)^2 - (y-Y)^2] \times \Theta(\mathbf{e}_z \cdot \mathbf{n}_D - \cos\alpha_D). \tag{3.1}$$

The Heaviside unit step function Θ is defined as $\Theta(x) \equiv (|x|+x)/(2|x|)$ and $\mu_T \equiv \mu_s+\mu_a$.

The total probability to measure singly scattered light is obtained by summing over all possible optical paths that can reach the detector area:

$$D_1(\mathbf{r}) = \int_0^\infty \int_0^\pi \int_0^{2\pi} d\xi\, d^2\Omega\, P(\xi,\boldsymbol{\Omega})\Theta(\rho_D - |\mathbf{R}-\mathbf{r}|) \times \Theta(\boldsymbol{\Omega}\cdot\mathbf{n}_D - \cos\alpha_D). \tag{3.2}$$

Let us discuss the meaning of the three factors in Eq. (3.2) separately. The first factor $P(\xi,\mathbf{\Omega})$ is related to the probability density that a photon scatters at location $\mathbf{r}_s+\boldsymbol{\xi}$ into the direction $\mathbf{\Omega}$. It is the product of the probability density not to scatter (or absorbed) between $\boldsymbol{\xi}=0$ and $\boldsymbol{\xi}$, then to scatter at location $\mathbf{r}_s+\boldsymbol{\xi}$ into the $\mathbf{\Omega}$ direction and then not to scatter again as it travels the remaining distance $|\mathbf{R}-\boldsymbol{\xi}-\mathbf{r}_s|$ to the detector:

$$P(\xi,\mathbf{\Omega}) \equiv \exp[-\mu_T\xi]\mu_s f_{\mathrm{HG}}(\mathbf{e}_z\cdot\mathbf{\Omega})\exp[-\mu_T|\mathbf{R}-\boldsymbol{\xi}-\mathbf{r}_s|]. \tag{3.3a}$$

For the conditional probability density to scatter into the $\mathbf{\Omega}$ direction we chose again the Henyey-Greenstein phase function $f_{\mathrm{HG}}(\mathbf{e}_z\cdot\mathbf{\Omega})\equiv(1/4\pi)(1-g^2)(1+g^2-2g\mathbf{\Omega}\cdot\mathbf{e}_z)^{(-3/2)}$.

The second factor in the integrand of Eq. (3.2) determines if photons miss or reach the detector area. The particular location at which the photon crosses the plane spanned by the detector area can be found from simple geometrical considerations

$$\mathbf{R}(\boldsymbol{\xi},\mathbf{\Omega}) = \mathbf{r}_s + \boldsymbol{\xi} + [\mathbf{n}_D\cdot(\mathbf{r}-\boldsymbol{\xi}-\mathbf{r}_s)/(\mathbf{\Omega}\cdot\mathbf{n}_D)]\mathbf{\Omega}. \tag{3.3b}$$

The third factor in Eq. (3.2), the second Θ function, guarantees that the angle of the incoming photon, $\cos^{-1}(\mathbf{\Omega}\cdot\mathbf{n}_D)$, is within the fiber's acceptance cone. We should mention that we count here the detected photons with equal weight and do not include here the precise details of the relationship between incoming angle and resulting photoelectric current generated by the detector. We also do not need here a factor $(\mathbf{\Omega}\cdot\mathbf{n}_D)$ which is required in flux based calculations based on the irradiance as discussed in Sec. IV [22].

To illustrate the general solution let us examine a special case of most interest to this work. We choose $\mathbf{n}_D=(0,0,1)$, $\mathbf{r}_s=(0,0,0)$ and monitor the detected light along the z axis, $\mathbf{r}=(0,0,z)$. In this case the three factors in the integrand simplify significantly. The first factor becomes

$$P(\xi,\mathbf{\Omega}) = \exp[-\mu_T\xi + (z-\xi)/(\cos\vartheta)]\mu_s f_{\mathrm{HG}}(\mathbf{\Omega}\cdot\mathbf{e}_z), \tag{3.4}$$

where ϑ is the polar angle of $\mathbf{\Omega}$ with regard to the z axis. The two unit-step functions reduce the upper integration limit to $\vartheta_{\max}(\xi)\equiv\min\{\tan^{-1}[\rho_D/(z\text{-}\xi)],\alpha_D\}$. The integrand does not depend on the azimuthal angle variable and we obtain

$$D_1(z) = 2\pi\mu_s\int_0^z d\xi\int_0^{\vartheta_{\max}(\xi)} \sin\vartheta\, d\vartheta \times\exp\{-\mu_T[\xi+(z-\xi)/\cos\vartheta]\}f_{\mathrm{HG}}(\vartheta). \tag{3.5}$$

This result is a generalization of the formula obtained in Refs. [15–20,22]. We should mention that the same result could be obtained formally from the first-order solution (in μ_s) to the Boltzmann equation for the irradiance $I(\mathbf{r},\mathbf{\Omega})$. If we integrate this irradiance over the detector area and those directions that are within the field of view of the detector, we obtain very quickly the nice integral, $\int_0^{\rho_D}2\pi\rho\, d\rho\int_0^{\alpha_D}2\pi\sin\vartheta\, d\vartheta\cos\vartheta\, I(\mathbf{r},\cos\vartheta)$, which due to the cylindrical symmetry simplifies to the single integral

$$D_1(z) = 2\pi\mu_s\int_0^{\alpha_D} d\vartheta\cos\vartheta\exp[-\mu_T z]\{1-\exp[-\mu_T M \times\tan(\vartheta/2)]\}f_{\mathrm{HG}}(\vartheta)/[\mu_T\tan(\vartheta/2)], \tag{3.6}$$

where $M\equiv\min\{\rho_D, z\tan(\vartheta/2)\}$. The expressions in Eqs. (3.5) and (3.6) are identical.

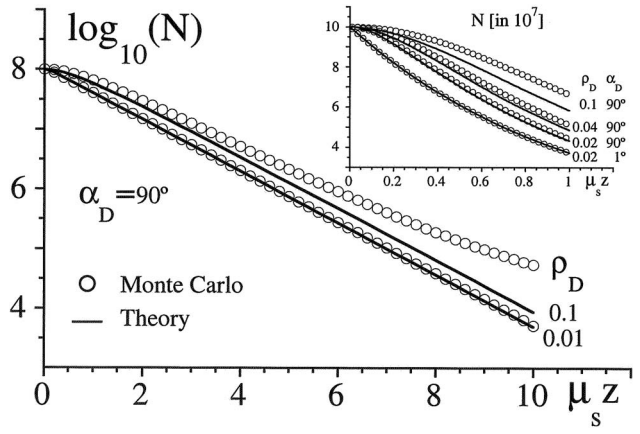

FIG. 4. Comparison of the few scattering theory with MC data (circles) for regimes I and II for two values of $\rho_D=0.01$ and 0.1 for $\alpha_D=90°$. Inset: The dependence of regime I on the detector radius ρ_D for $\alpha_D=90°$ and 1°. Note the linear intensity scale. ($N=10^8$ photons, $\mu_s=1$, $\mu_a=0$, $g=0.9$, and $W=10$.)

Let us first examine the range of validity of this solution. In Fig. 4 we have graphed the detected light distribution as a function of z for a medium of width $W=10$. The circles are the data of the Monte Carlo simulation and the continuous lines are the analytical results from Eqs. (3.1) and (3.6), $D_0(z)+D_1(z)$. For small values of ρ_D and α_D the few scattering theory works very well and predicts correctly the behavior in regime I (enlarged in the inset) and the exponential decay region II. As ρ_D or α_D is increased, more than just single scattering events are detected leading to a larger intensity than predicted by this theory. It is important to note that while this particular theory predicts an exponential decay with the rate $\mu_s+\mu_a$, the Monte Carlo data suggest that the actual exponential rate can be much less and depends on the angle α_D as well as the radius ρ_D.

In the inset we show on a linear scale the intensity decay for very short distances for three different values of ρ_D. For small values of α_D and ρ_D the detected light is dominated by unscattered light leading to a nearly immediate exponential decay, whereas if the detector is either sufficiently wide or has a sufficiently wide field of view, we note deviations such as doubly scattered light can also be detected. As suggested above the details of this region also depend on the anisotropy g.

After this numerical discussion, let us explore the limiting cases of the expression Eq. (3.6). One could incorrectly expect that for very short distances the nonscattered light given by $D_0(z)=\exp[-\mu_T z]$ dominates, leading to the Beer-Lambert exponential decay law with decay constant μ_T and that only after a characteristic distance deviations from the

exponential decay due to singly scattered light occur. However, the first two terms of the Taylor expansion of $D_0(z)+D_1(z)=1-\mu_T[1-\mu_s/\mu_T 2\pi\int_0^{\alpha_D} d\vartheta \sin\vartheta f_{\mathrm{HG}}(\vartheta)]\ z$ suggest that, depending on g and the angle α_D, the initial slope can be significantly smaller than μ_T. In fact the initial decay of $D_0(z)+D_1(z)$ could be even quadratic, as the linear term in z can vanish if either g is close to unity or α_D is very large, leading in both cases to $2\pi\int_0^{\alpha_D} d\vartheta \sin\vartheta f_{\mathrm{HG}}(\vartheta)\approx 1$. This rather sensitive property could be exploited to use the scattering data to reconstruct g from very thin slabs and also to examine properties of the phase function.

Let us complete this section with two comments about the range of validity of the few scattering theory. The theory takes only those photons into account that scatter at most once before hitting the detector. The theory therefore underestimates the signal if doubly and multiply scattered photons enter the detector as well. We compared the theory with the Monte Carlo data for various anisotropy parameters g and found that for $g=0$ the theory is extremely good and valid for the largest *s-d* distances. This makes sense, as for the opposite limit of g close to 1 as well as g close to -1, the multiply scattered photons stay close to the optical axis and would unavoidably also pass through the detector, making the theory invalid. We also found that the decay rate is largest for fully isotropic scattering ($g=0$), as multiply scattered photons can most effectively avoid being detected.

IV. DIFFUSION THEORIES FOR REGIME IV

As the derivation of the results for undirected laser sources can be found in various publications [13,35,36], we just sketch here the final expressions for our angularly collimated source. The diffusion approximation depends only on two parameters to characterize the medium, the diffusion coefficient, $D\equiv[\mu_a+(1-g)\mu_s]^{-1}/3$, and the absorption coefficient μ_a. The irradiance is approximated by its two velocity moments, $I(\mathbf{r},\mathbf{\Omega})\approx(1/4\pi)\phi(\mathbf{r})+(3/4\pi)\mathbf{\Omega}\cdot\mathbf{J}(\mathbf{r})$, where the fluence $\phi(\mathbf{r})\equiv\int d^2\Omega\, I(\mathbf{r},\mathbf{\Omega})$ and the flux $\mathbf{J}(\mathbf{r})\equiv\int d^2\Omega\,\mathbf{\Omega}\, I(\mathbf{r},\mathbf{\Omega})$. The light measured in the opening of the detection fiber can be obtained via

$$D_{\mathrm{diff}}(z)=\int 2\pi\rho\, d\rho \int d^2\Omega(\mathbf{n}_D\cdot\mathbf{\Omega})I(\mathbf{r},\mathbf{\Omega}), \tag{4.1}$$

where the angular integral covers the opening cone of the fiber with angle α_D and the integration over the cylindrical coordinate ρ extends from 0 to the radius of the fiber ρ_D. We should note that in contrast to the theory from Sec. II, the diffusion theory predicts the light independent of the measurement and if light passes through the detection area multiple times, the intensity would be overestimated compared to the measured one. As we will see below, the regime of validity of the diffusion theory depends crucially on the size of ρ_D.

If we use Fick's law, relating the flux to the fluence via $\mathbf{J}(\mathbf{r})=-D\nabla\phi(\mathbf{r})$, we can perform the integral over the angular cone, $\int d^2\Omega(\mathbf{n}_D\cdot\mathbf{\Omega})=\pi\sin^2\alpha_D$ and $\int d^2\Omega(\mathbf{n}_D\cdot\mathbf{\Omega})\Omega_z=2\pi/3(1-\cos^3\alpha_D)$, and we are left with the integration over the surface area of the fiber

$$D_{\mathrm{diff}}(z)=\tfrac{1}{4}\sin^2\alpha_D\int 2\pi\rho\, d\rho\,\phi(\mathbf{r}) - (1-\cos^3\alpha_D)/2D\int 2\pi\rho\, d\rho\,\partial\phi(\mathbf{r})/\partial z. \tag{4.2}$$

There are two different geometries for which analytical solutions for the fluence can be obtained using the method of image charges [37]: The slab geometry and (its limiting case) the semi-infinite medium. The fluence for a slab of width W is given by

$$\phi_{\mathrm{slab}}(\mathbf{r})=\sum_{m=-\infty}^{\infty}[S_1(m)+S_2(m)+S_3(m)+S_4(m)], \tag{4.3}$$

where the four functions are given by

$$S_1(m)\equiv[1/(4\pi D)]\exp[-\kappa\xi^-(\rho,m,z)]/\xi^-(\rho,m,z)^{-1}, \tag{4.4a}$$

$$S_2(m)\equiv-[1/(4\pi D)]\exp[-\kappa\xi^+(\rho,m,z)]/\xi^+(\rho,m,z)^{-1}, \tag{4.4b}$$

$$S_3(m)\equiv[3/(4\pi)][z+2m(W+2z_0)]\exp[-\kappa\xi^-(\rho,m,z)]\times[\kappa\xi^-(\rho,m,z)^{-2}+\xi^-(\rho,m,z)^{-3}], \tag{4.4c}$$

$$S_4(m)\equiv[3/(4\pi)][z+2z_0+2m(W+2z_0)]\exp[-\kappa\xi^+(\rho,m,z)]\times[\kappa\xi^+(\rho,m,z)^{-2}+\xi^+(\rho,m,z)^{-3}]. \tag{4.4d}$$

Here we have used the following abbreviations: $\kappa\equiv\sqrt{[\mu_a/D]}$, $\xi^-(\rho,m,z)\equiv\sqrt{\{\rho^2+[z+2m(W+2z_0)]^2\}}$, and $\xi^+(\rho,m,z)\equiv\sqrt{\{\rho^2+[z+2z_0+2m(W+2z_0)]^2\}}$. The length $z_0\equiv 2.1D$ is related to the location of the first image charge used to solve the diffusion theory with the approximate boundary condition $\phi_{\mathrm{slab}}(x,y,z=-2.1D)=0$ and $\phi_{\mathrm{slab}}(x,y,z=W+2.1D)=0$.

The general solution Eq. (4.3) for the fluence for the slab can be interpreted if we analyze its limiting cases. For example, the semi-infinite medium is obtained for $W\to\infty$ and represented by a comparably easier formula:

$$\phi_{\mathrm{semi}}(\mathbf{r})=S_1(m=0)+S_2(m=0)+S_3(m=0)+S_4(m=0). \tag{4.5}$$

The first term is identical to the fluence for an undirected source in an infinite medium, $S_1(m=0)=\phi_{\mathrm{inf}}(\mathbf{r})=[1/(4\pi D)]\exp[-\kappa r]/r$. The third term, $S_3(m=0)=[3/(4\pi)]z\exp[-\kappa r][k/r^2+1/r^3]$ is associated with the correction due to the directionality of the source. The sum of the second term, $S_2(m=0)=\phi_{\mathrm{inf}}(\mathbf{r}+2z_0\mathbf{e}_z)$, and the fourth term are the fluences due to the image source located at $\mathbf{r}=-2z_0\mathbf{e}_z$ reflecting the approximate mathematical boundary condition $\phi_{\mathrm{semi}}(x,y,z=-2.1D)=0$.

Note that if we choose $z=W$ the prediction of the slab theory would be based on only a *single* photon passage through the detector, suggesting that in certain regimes this model could be reasonable to predict experimental data for a

semi-infinite system where the perfectly absorbing detector is inside the medium.

Before we discuss the transition into this diffusive regime, let us remark that—quite surprisingly at first—for short source-detector spacings (of the order of $1/\mu'$) the predicted detected light is identical for $\phi_{\text{slab}}(\mathbf{r})$ and $\phi_{\text{semi}}(\mathbf{r})$. This is true even if $z=W$ and we compare the distribution of a very thin slab with a semi-infinite medium. In fact, the two theories differ only for large distances. This unexpected agreement can be understood as follows. The light that misses the detector area leaves the medium for the slab geometry, whereas for the semi-infinite medium it could turn around due to scattering. If this returned light happens to enter the detector area we would expect a different result between $\phi_{\text{slab}}(\mathbf{r})$ and $\phi_{\text{semi}}(\mathbf{r})$. However, once the light crosses the (x,y) plane at z, it must turn around by 180° to become detectable. On average each photon requires a radius of the inverse transport length $1/\mu'$ in order to turn around. If $z<1/\mu'$, however, the photons would exit at the boundary at $z=0$ and cannot return to the detector. As a consequence those photons that could make a difference between the slab and semi-infinite geometry cannot reach the detector. We should point out that this finding, however, does not contradict the above statement that $\phi_{\text{semi}}(\mathbf{r})=\lim_{(W\to\infty)}\phi_{\text{slab}}(\mathbf{r})$. A similar argument was used in Sec. II to show why $\Xi\approx 0$ close to the surfaces.

In Fig. 5 we compare the different diffusion theories with two types of Monte Carlo simulations for various detection parameters. The continuous lines are the prediction of the slab theory; the dashed lines correspond to the semi-infinite medium. The crosses are the Monte Carlo data representing a real (perfectly) absorbing detector in which only the first passage through the detection area is counted. The circles permit multiple passage and therefore permit multiple counting of photons. The latter is associated with an ideal detector whose presence has no impact on the light distribution. For large $\rho_D(=50)$, shown on a linear scale in Fig. 5(a), the difference between both detector readings is significant; for instance, for region $z<10$ we find that the number of photons that pass through the detector exceeds the total number of injected photons. In this particular case the maximum degree of destructiveness Ξ exceeded 78% at $z=W/2$. As mentioned above, the diffusion theories permit a multiple detection of the same photon, so the agreement with the corresponding Monte Carlo data is remarkably good for small *s-d* spacings, but bad for the data based on a single passage.

In Fig. 5(b) we show on a logarithmic scale the data for other detector areas. For $\rho_D<10$, the MC data for both types of detectors are nearly identical. We see that, roughly halfway into the medium, the two diffusion-type theories predict similar data, whereas for locations $z>W/2$ the photons that can exit at $z=W$ lead to a lower number of detectable photons compared to those of a semi-infinite slab. For smaller fiber radii ρ_D, however, an agreement with the diffusion theory would require larger spacings z.

V. COMPARISON WITH EXPERIMENTAL DATA

Let us briefly describe the experimental setup. We have used two laser systems: A temperature controlled (ILX LDT-5412) diode system (LDX-3525) lasing with about 80 mW at around 560 nm and a HeNe laser (Spectra-Physics Stabilite 124B) lasing at 30 mW. As the medium, we chose diluted solutions of nondairy creamer (Concepts), which is basically corn syrup solids and soybean oil, in water with a concentration of about 0.7778 g/L in our rectangular glass container of $20\times 20\times 50$ cm. We believe that the tank is large enough to neglect boundary effects. The central piece of our setup is a computer controlled translation stage that permits us to vary the location of the optical detection fiber inside the medium with an accuracy of less than 25 μm inside an area of 85×55 cm. To maximize our photon collection efficiency while maintaining control over the direction we used an Eska acrylic optical fiber (Edmonds) with radius of $\rho_D=750$ μm and a numerical aperture of 0.51, corresponding to a maximum acceptance angle of $\alpha_D=22°$ in water and for comparison [38] we also used Silica core multimode fibers (Thorlab) with diameters of 0.91 mm (BFL 22-910) and 0.6 mm (BFL 37-600). The fiber is connected to a wide area photo receiver (NewFocus 2031), whose photoelectric output voltage is sent into an amplifier (SR 250) before it is recorded using LabView, which also controls the two stepper motors for the

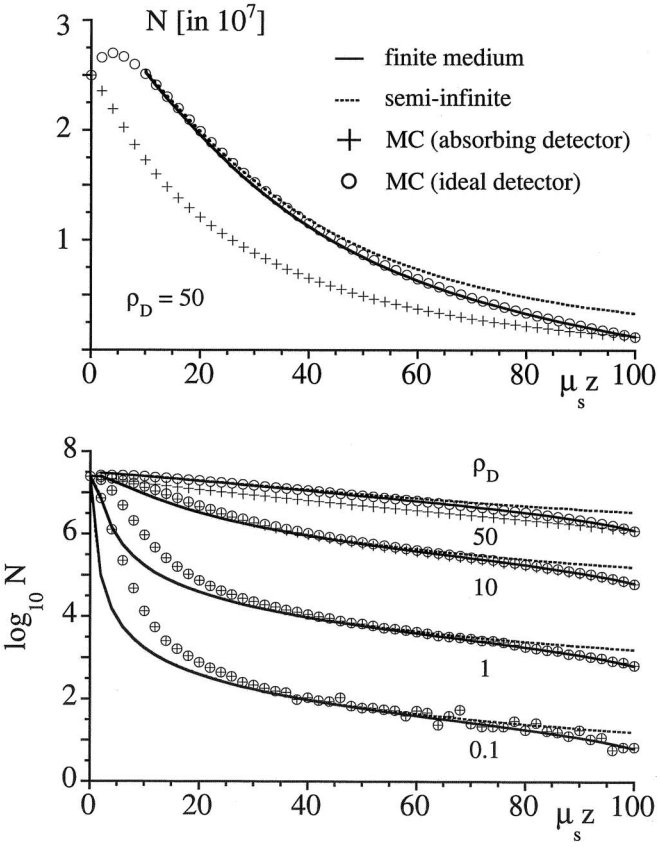

FIG. 5. Comparison of the slab and semi-infinite diffusion theory with MC data for absorbing and ideal detectors. The top figure on a linear scale shows that the diffusion theory can predict the data of a nonabsorbing detector very well for remarkably short distances, if the radius of the detection fiber is sufficiently large. The bottom figure compares the data on a logarithmic scale for various fiber radii. ($N=2.5\times 10^7$ photons, $\mu_s=1$, $\mu_a=0$, $g=0.9$, and $W=100$.)

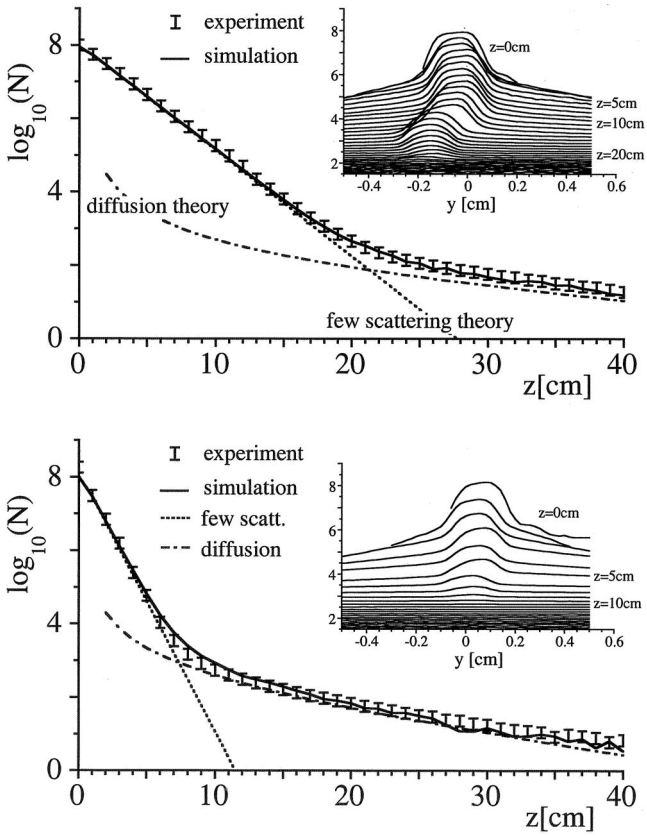

FIG. 6. Experimental data (bars) compared to MC data (line) (based on 10^8 photons) using anisotropy $g=0.8$, $\mu_s=0.66$ cm^{-1}, and $\mu_a=0.01$ cm^{-1}. The dotted graph is the few-scattering theory [based on the analytical solutions of Eqs. (3.1) and (3.6)] and the dashed line is the slab diffusion theory [based on Eqs. (4.1)–(4.4)]. The medium was a water nondairy creamer solution with a concentration of 777.8 mg/l. The detection fiber had a numerical aperture of NA=0.51 with $\rho_D=750$ μm. The inset shows the beam profiles for various distances z. (Top) Dilute medium and (bottom) less dilute medium.

translation stage. We used several neutral density filters to attenuate the signal close to the source to obtain the required dynamic intensity range and rescaled the data accordingly.

In order to obtain the data on axis, we have scanned for a given location z in the transverse direction to measure the beam profile as a function of y. A typical example of these scans is shown in the inset in Fig. 6(a). The He Ne laser beam has a $1/e^2$-Gaussian waist of 1.1 mm as we verified in a separate measurement using a much smaller fiber (with diameter of 0.125 mm). As the diameter $2\rho_D$(=1.5 mm) of our main detection fiber exceed 1.1 mm, the detected waist is larger than the true beam width. The shift of the center location of the beam with increasing z is associated with a change of the neutral density filters which slightly redirect the beam. We note that the decrease in the beam's signal strength is more associated with an amplitude attenuation than a widening of the beam. The beam profiles show that there are at least two regimes in z; for small spacings the beam is clearly visible above the background, whereas for $z>20$ cm the background exceeds the beam's strength. This value correlates nicely with the extension of the exponential decay regime II.

The bars in Fig. 6(a) show the maximum value of each beam profile as a function of the fiber location z. As predicted in Sec. II, the different regimes are clearly visible. For comparison, we have also indicated by the continuous curve the predictions by the Monte Carlo simulation based on $N=10^8$ photons and taking the nonzero initial beam widths into account. The experimental data (normalized to match the MC data at $z=20$ cm) are best matched by $\mu_s\approx 0.66$ cm^{-1}, $\mu_a\approx 0.01$ cm^{-1}, and $g=0.8$, showing that, at 633 nm, the nondairy creamer is a highly forward scattering substance where the scattering strength is at least 50 times that of the absorption. We found that the MC data for the on-axis signal strength are quite sensitive to changes in the scattering parameters μ_s, μ_a, and g, which is promising for more optimized reconstruction schemes which we will discuss elsewhere.

For comparison, we have also included the predictions of the two analytical theories according to Eqs. (3.1) and (3.6) for the few scattering theory and Eqs. (4.2)–(4.4) for the diffusion theory. We note that the two theories were not normalized independently, both are scaled corresponding to the same source strength. Despite the relatively large value of g, the few scattering theory is not so bad, whereas the diffusion theory would describe the signal only for much larger distances z exceeding the size of our tank.

To make contact with the diffusion regime, we have repeated the measurement for a medium in which we have increased the concentration of the scattering nondairy creamer. The results are shown in Fig. 6(b). In this case, the diffusion theory for the slab ($\mu_s\approx 1.63$ cm^{-1}, $\mu_a\approx 0.03$ cm^{-1}, and $g=0.8$) matches the experimental data already for much shorter distances $z\approx 10$ cm. This value agrees again with the distance at which the narrow beam profile dives into the background value, as shown in the inset.

VI. SUMMARY AND OUTLOOK

In this work, we have examined the light distribution for scattered light along the beam axis and found four characteristic regimes depending on the source detector spacing. We simulated the experimental signal using Monte Carlo data and we tested the accuracy of various approximate but analytical theories. We point out that—in addition to the optical parameters of the medium—also the parameters characterizing the detection fiber can determine the range of validity of these theories. As the data were taken along the optical axis and a nearly complete removal of light from the system is unavoidable, we had to examine also the impact of the measurement process on the distribution of the light. As analytical theories are often essential for efficient image inversion schemes, it is necessary to understand under which conditions the on-axis light measurements are destructive and limit the validity of approximate analytical approaches that usually do not take a perfectly absorbing detector into account. We defined a numerical degree of destructiveness Ξ to compute a possible error for those theoretical descriptions

that cannot take the effect of the measurement into account. These errors can be significant for large fiber openings and acceptance angles.

In future work, we will continue to explore the nondiffusive regimes I, II, and III with regard to the light distribution off the optical axis as well as for fiber alignments that are not parallel to the optical axis as discussed here. Our preliminary results reported here suggest that the on-axis data in regions II and III are quite sensitive to the optical scattering parameters. We should mention that the spatial extent of all four regimes depends on the medium characteristics as well as the detection parameters. We will explore how the nontrivial on-axis signal discussed here can be used to accurately and systematically determine the scattering parameters. These studies will also test the validity of the particular scattering phase function used in this work [34]. One could also replace the nondairy creamer scattering medium with a solution of water with latex microspheres of identical radii with precisely known optical properties in order to have more accurate comparisons of the quality of our on-axis method.

A better understanding of regimes II and III would also open new avenues for improved imaging. In medical endoscopy, e.g., a small spacing between the fiber source and detector is unavoidable and diffusion-based theories fail to reliably predict the light distributions. In non-diffusive media such as narrow biotissues, regimes II and III determine transillumination as well as reflective measurements. The diffusion theory is also known to become less reliable when the absorption is too large [39], but significant progress in bio-optical imaging was reported in the past few years [40–46].

ACKNOWLEDGMENTS

We appreciate various useful discussions on the experimental aspects as well as numerous equipment loans from Professor B.K. Clark. We thank Professor G.H. Rutherford for useful discussions, J. Dunham for designing and building the translation stage, Professor D. Cedeno the photospectrometric and goniometric data for our milk suspensions, and Professor D. Marx for help with preparing our optical fibers. This work has been supported by the NSF. We also acknowledge support from the Research Corporation for Cottrell Science Awards and BLV.

[1] J. J. Duderstadt and L. J. Hamilton, *Nuclear Reactor Analysis* (Wiley, New York, 1976).
[2] A. Ishimaru, *Wave Propagation and Scattering in Random Media* (Academic, New York, 1978), Vols. 1 and 2.
[3] V. V. Tuchin, Phys. Usp. **40**, 495 (1997).
[4] W. R. Hendee, Rev. Mod. Phys. **71**, S444 (1999).
[5] *The Essential Physics of Medical Imaging*, edited by J. T. Bushberg, J. A. Seibert, E. M. Leidholdt, Jr., and J. M. Boone, 2nd ed., (Lippincott Williams & Wilkins, Philadelphia, 2002).
[6] *Nondestructive Evaluation: Theory, Techniques, and Applications*, edited by P. J. Shull (Dekker, New York 2002).
[7] K. M. Yoo, F. Liu, and R. R. Alfano, Phys. Rev. Lett. **64**, 2647 (1990).
[8] H. J. van Staveren, C. J. M. Moes, Jan van Marle, S. A. Prahl, and M. J. C. van Gemert, Appl. Opt. **30**, 4507 (1991).
[9] J. B. Fishkin, S. Fantini, M. J. vande Ven, and E. Gratton, Phys. Rev. E **53**, 2307 (1996).
[10] C. K. Hayakawa, B. Y. Hill, J. S. You, F. Bevilacqua, J. Spanier, and V. Venugopalan, Appl. Opt. **43**, 46777 (2004).
[11] S. Menon, Q. Su, and R. Grobe, Phys. Rev. Lett. **94**, 153904 (2005).
[12] J. S. You, C. K. Hayakawa, and V. Venugopalan, Phys. Rev. E **72**, 021903 (2005).
[13] E. L. Hull and T. H. Foster, J. Opt. Soc. Am. A **18**, 584 (2001).
[14] F. Bevilacqua and C. Deoeursinge, J. Opt. Soc. Am. A **16**, 2935 (1999).
[15] A. Deepak and M. A. Box, Appl. Opt. **17**, 2900 (1978).
[16] A. Deepak and M. A. Box, Appl. Opt. **17**, 3169 (1978).
[17] A. Deepak, U. O. Farrukh, and A. Zardecki, Appl. Opt. **21**, 439 (1982).
[18] W. G. Tam and A. Zardecki, Appl. Opt. **21**, 2405 (1982).
[19] A. Zardecki and W. G. Tam, Appl. Opt. **21**, 2413 (1982).
[20] L. Wind and W. W. Szymanski, Meas. Sci. Technol. **13**, 270 (2002).
[21] S. Del Bianco, F. Martelli, and G. Zaccanti, Phys. Med. Biol. **47**, 4131 (2002).
[22] S. Fantini, M. A. Franceschini, and E. Gratton, Appl. Opt. **36**, 156 (1997).
[23] S. Menon, Q. Su, and R. Grobe, Phys. Rev. E **67**, 046619 (2003).
[24] S. Menon, Q. Su, and R. Grobe, Phys. Rev. E **68**, 046614 (2003).
[25] M. Keijzer, S. L. Jacques, S. A. Prahl, and A. J. Welch, Lasers Surg. Med. **9**, 148 (1989).
[26] L. H. Wang and S. L. Jacques, J. Opt. Soc. Am. A **10**, 1746 (1993).
[27] L. H. Wang and S. L. Jacques, Comput. Methods Programs Biomed. **47**, 131 (1995).
[28] S. A. Prahl, M. Keijzer, S. L. Jacques, and A. J. Welch, SPIE Dosimetry of Laser Radiation in Medicine and Biology **5**, 102 (1989).
[29] S. Behin-Ain, T. van Doorn, and J. R. Patterson, Med. Phys. **29**, 125 (2002).
[30] A. H. Hielscher, A. Y. Bluestone, G. S. Abdoulaev, A. D. Klose, J. Lasker, and M. Stewart, Disease Markers **18**, 313 (2002).
[31] W. H. Press, B. P. Flannery, S. A. Teukolsky, and T. T. Vetterling, *Numerical Recipes* (Cambridge University Press, New York, 1986).
[32] J. Spanier and E. M. Gelbard, *Monte Carlo Principles and Neutron Transport Problems* (Addison-Wesley, Reading, MA, 1969).
[33] S. Kirkpatrick and E. Stoll, J. Comput. Phys. **40**, 517 (1981).
[34] J. R. Mourant, J. Boyer, A. H. Hielscher, and I. J. Bigio, Opt. Lett. **21**, 546 (1996).
[35] B. B. Das, F. Liu, and R. R. Alfano, Rep. Prog. Phys. **60**, 227

(1997).
[36] M. C. W. van Rossum and T. M. Nieuwenhuizen, Rev. Mod. Phys. **71**, 313 (1999).
[37] J. Ripoll and V. Ntziachristos, J. Opt. Soc. Am. A **20**, 1103 (2003).
[38] V. Venugopalan, J. S. You, and B. J. Tromberg, Phys. Rev. E **58**, 2395 (1998).
[39] D. J. Durian and J. Rudnick, J. Opt. Soc. Am. A **14**, 235 (1997).
[40] J. Ripoll, V. Ntziachristos, J. P. Culver, D. Pattanayak, A. G. Yodh, and M. Nieto-Vesperinas, J. Opt. Soc. Am. A **18**, 821 (2001).
[41] R. Elaloufi, R. Carminati, and J. J. Greffet, J. Opt. A, Pure Appl. Opt. **4**, S103 (2002).
[42] J. Ripoll, R. B. Schulz, and V. Ntziachristos, Phys. Rev. Lett. **91**, 103901 (2003).
[43] R. Elaloufi, R. Carminati, and J. J. Greffet, J. Opt. Soc. Am. A **20**, 678 (2003).
[44] M. Xu and R. R. Alfano, Phys. Rev. Lett. **95**, 213901 (2005).
[45] M. Xu and R. R. Alfano, Opt. Lett. **30**, 3051 (2005).
[46] J. Ripoll, D. Yessayan, G. Zacharakis, and V. Ntziachristos, J. Opt. A, Pure Appl. Opt. **22**, 546 (2005).